International Journal of Heat and Mass Transfer 52 (2009) 4160–4174

Contents lists available at ScienceDirect

International Journal of Heat and Mass Transfer

journal homepage: www.elsevier.com/locate/ijhmt

Off-centre binary collision of droplets: A numerical investigation

N. Nikolopoulos, A. Theodorakakos, G. Bergeles *

Department of Mechanical Engineering, Nat. Technical University of Athens, 15310 Zografos, Greece

ARTICLE INFO

Article history:
Received 28 September 2008
Accepted 22 April 2009
Available online 25 May 2009

Keywords:
Binary collision
Ligament
Satellite droplet formation
Volume of Fluid Method

ABSTRACT

The paper presents results from a numerical investigation of the non-central binary collision of two equal size droplets in a gaseous phase. The flow field is two phase and three dimensional; the investigation is based on the finite volume numerical solution of the Navier–Stokes equations, coupled with the Volume of Fluid Method (VOF), expressing the unified flow field of the two phases, liquid and gas. A recently developed adaptive local grid refinement technique is used, in order to increase the accuracy of the solution particularly in the region of the liquid–gas interface. The reliability of the solution procedure is tested by comparing predictions with available experimental data. The numerical results predict the collision process of the two colliding droplets (permanent coalescence or separation) and in the case of separation the formation and the size of the satellite droplets. The time evolution of the geometrical characteristics of the ligament, for various Weber numbers and impact parameters, is calculated and details are shown of the velocity and pressure fields particularly at the ligament pinch off location not hitherto available. Gas bubbles due to collision are trapped within the liquid phase as it has also been observed in experiments and their volume is calculated.

1. Introduction

Binary droplet collision is appearing in raindrop formation and in various spray processes, especially in internal combustion engines. The first studies on droplet collision, using water droplets in air at atmospheric pressure, have been conducted because of meteorological interest by Adam et al. [1]. They focused attention on the aerodynamic environment of the event and on the outcome of the collisions. Park [2] produced collisions between streams of water droplets traveling in still air and showed pictorially that near head-on collision between pairs of equally sized droplets of 700 μm, resulted in stable coalescence, while off-centre collision at the same relative velocity resulted in a transient coalescence and finally in separation. Brazier-Smith et al. [3] conducted similar experiments to [2] in still air, whilst Ashgriz and Poo [4] developed models for predicting the boundary between the coalescence and separation regimes.

Faeth [5], O'Rouke and Bracco [6] emphasized the importance of droplet collision phenomena occurring within dense sprays and recognized the significance of the rheological properties of the droplets (i.e. hydrocarbons vs. water). As reported by Qian and Law [7] for water droplets, for head-on collisions at atmospheric pressure bounce is not observed; for the same conditions however, the collision outcome between hydrocarbon droplets may result to bouncing.

Jiang et al. [8] provided a comprehensive quantitative assessment of droplet collisions of hydrocarbon droplets (heptane, decane, dodecane, tetradecane and hexadecane), and later Qian and Law [7] extended these investigations to include the effects of ambient pressure, density, viscosity and impact parameter (characterizing off-centre binary collisions). In each of the above studies, mono-disperse streams of droplets were made to collide at various angles. The following collision regimes were found with increasing Weber number; droplet bouncing, stable droplet coalescence, unstable droplet coalescence and droplet stretching separation, [7,8].

Estrade et al. [9] published information about the number of satellite droplets, their sizes and velocities produced by bouncing collisions. Moreover, they also developed a model for predicting the boundary between the bouncing and the coalescence regimes. Brazier-Smith et al. [3] carried out experiments on binary water droplet collisions and developed the threshold of the stability of water droplets against separation, while Arkhipov et al. [11] obtained a relation for the impact parameter separating stable coalescence from stretching separation. Willis and Orme [12] conducted experiments of droplet collisions in a vacuum, devoid of aerodynamic effects, focusing on the role of viscosity in the evolution of the collision phenomenon. Brenn et al. [10] produced a monogram for the various collision regimes and for the number of satellite droplets formed during droplet collision depending on the Weber

* Corresponding author. Address: Department of Mechanical Engineering, Nat. Technical University of Athens, 5 Heroon Polytechniou, Zografos, 15310 Athens, Greece. Tel.: +30 2107721058; fax: +30 2107723616.
E-mail addresses: niknik@fluid.mech.ntua.gr (N. Nikolopoulos), andreas@fluid.mech.ntua.gr (A. Theodorakakos), bergeles@fluid.mech.ntua.gr (G. Bergeles).

0017-9310/$ - see front matter © 2009 Elsevier Ltd. All rights reserved.
doi:10.1016/j.ijheatmasstransfer.2009.04.011

Nomenclature

B	impact parameter, (= x/D_o)
D_o	initial droplet's diameter
f_σ	force due to surface tension
L_1	maximum elongation of coalesced mass
L_2	maximum elongation of ligament or satellite droplet
Re	Re number, (= $\rho_{liq} D_o (2 U_o)/\mu_{liq}$)
t	time
$\vec{T}$	stress tensor
T	non-dimensional time, (= tU_o/D_o)
U_o	initial droplet's impact velocity
$\vec{u}$	velocity
x	the projection of the separation distance between the droplet centres in the direction normal to that of U_o
X	X-axis of computational field
Y	Y-axis of computational field
Z	Z-axis of computational field
We	We number, (= $\rho_{liq} D_o (2 U_o)^2/\sigma$)
w_2	maximum width of ligament or satellite droplet

Greek symbols

α	volume of fluid (also noted as indicator function)
κ	curvature (m^{-1})
μ	dynamic viscosity (kg/m s)
ρ	density (kg/m^3)
σ	surface tension (N/m)

Subscripts

gas	gas phase
liq	liquid phase
tot	total

number and impact parameter. In the same work results are presented of the characteristics of the formed ligament and satellite droplet diameter. These results have been obtained following a linear stability analysis of the filament formed after collision which agreed quite well with the experimental results of Ashgriz and Poo [4], who showed that for the same *Weber* number of the two colliding droplets, the number of satellite droplets resulting from the droplet separation increases with the increase of the impact parameter.

Studies on the numerical simulation of droplet binary collision are relatively few. The front tracking method for multi-fluid methods developed by Unverdi [13] and discussed by Unverdi and Tryggvason [14–15], was used by Nobari et al. [16] in axi-symmetric formulation for central collision; the method was able to capture the features of bouncing, coalescence and reflexive separation with up to one satellite droplet formed, by prescribing the rupture time of the inter-drop film. The methodology was extended by Nobari and Tryggvason [17] for three dimensional simulations of droplet collisions, but for a low density and viscosity ratio between surrounding gas and droplet 40 and 20 and on a fixed numerical grid ($32 \times 32 \times 64$). In the present simulations the density ratio of liquid to gas phase is much higher and equal to 610 with a viscosity ratio of 129.

Mashayek et al. [18] studied the coalescence collision of two droplets in axi-symmetric coordinates, using a Galerkin finite element method coupled with the spline-flux method for the free surface tracking. Lafaurie et al. [19] used the SURFER method, lattice gas models were used by Drtina et al. [20], Schelkle and Frohn [21,22] in three dimensions, whilst Rieber and Frohn used VOF methodology [23].

Inamuro et al. [24] neglecting the effect of the gas on the droplet collision, presented a lattice Boltzmann simulation of binary droplet collisions in a system with a density ratio of 50 and compared the numerically predicted collision consequences with the inter-regime boundaries given by the model developed by Ashgriz and Poo [4]. In addition they simulated the mixing process of equal-sized droplets, during separating collisions for various impact parameters at We = 80, for the given density ratio. Recently, Pan and Kazuhiko [25] using the implicit continuous-fluid Eulerian method coupled with the level set methodology for a single phase in a fixed uniform mesh system, simulated the three major regimes of binary collision (bouncing, coalescence and separation), both for water and hydrocarbon droplets. Their numerical results suggest that the mechanism of bouncing collision is governed by the macroscopic dynamics while the mechanism of coalescence is related to the microscopic dynamics. By their simulations, it is confirmed that in the case of large impact parameter cases, the capillary-wave instability is the controlling mechanism for the satellite droplets formation, whereas in the case of an intermediate impact parameter, the effects of twisting and stretching due to the angular momentum and the inertia of the colliding droplets are significant for the satellite droplet formation.

Finally, a methodology for the prediction of the borders between the various collision outcome regimes has been undertaken by Munnannur and Reitz [26]. They recently formulated a new model, including bouncing, coalescence and separation as outcomes. This model predicts not only the outcome of the collision, but also the post-collision characteristics such as droplet sizes, velocities and spatial distribution of droplets in the case of polydisperse streams of droplets, under the assumption that the satellite droplets resulting from fragmentation are uniform in size and velocity.

The present investigation studies numerically the off-centre collision of hydrocarbon droplets for various Weber and Reynolds numbers. The Navier–Stokes equations with the introduction of a volumetric force due to surface tension effects are solved numerically by the finite volume methodology; the numerical solution employs a new adaptive local grid refinement technique, whilst VOF methodology is used for the tracking of the liquid–gas interfaces.

Results are presented in which first the reliability of the methodology is established by comparing predictions with reliable published experimental data. After that, new findings are presented regarding the collision mechanism (coalescence or separation) of the two colliding droplets.

2. The mathematical problem

The flow induced by the non-central binary collision of two equal sized droplets is considered as three-dimensional, incompressible and laminar; the two-phase flow (phase 2 is the liquid phase, and phase 1 is the surrounding gas phase) is mathematically expressed by the Navier–Stokes equations and the continuity equation. For identifying each phase separately a volume fraction, denoted by α, is introduced following the Volume of Fluid Method (VOF) of Hirt and Nichols [27]. In the VOF method the volume fraction α is defined as:

$$\alpha = \frac{\text{Volume of liquid phase}}{\text{Total volume of the control volume}} \quad (1)$$

The values of density ρ and viscosity μ are calculated using linear interpolation between the values of the two phases weighted with the volume fraction α:

$$\rho = \alpha\rho_{liq} + (1-\alpha)\rho_{gas}$$
$$\mu = \alpha\mu_{liq} + (1-\alpha)\mu_{gas} \quad (2)$$

where the α-function is equal to:

$$a(x,t) = \begin{cases} 1, & \text{for a point}(x,t)\text{inside liquid phase} \\ 0, & \text{for a point}(x,t)\text{inside gas phase} \\ 0 < \alpha < 1, & \text{for a point}(x,t)\text{inside the} \\ & \text{transitional area between the two phases} \end{cases} \quad (3)$$

The transport equation for the volume fraction is

$$\frac{D\alpha}{Dt} = \frac{\partial\alpha}{\partial t} + u \cdot \nabla a = 0 \quad (4)$$

The momentum equations expressing both phases are written in the form

$$\frac{\partial(\rho\vec{u})}{\partial t} + \nabla \cdot (\rho\vec{u} \otimes \vec{u} - \vec{T}) = \rho\vec{g} + \vec{f}_\sigma \quad (5)$$

where $\vec{T}$ is the stress tensor, $\vec{u}$ is the velocity and f_σ is the volumetric force due to surface tension. The volumetric force f_σ is equal to

$$f_\sigma = \sigma \cdot \kappa \cdot (\nabla a),$$

where σ is the numerical value of the surface tension (for immiscible fluids the value is always positive) and κ is the curvature of the interface region as calculated by Brackbill et al. [28].

3. The numerical solution procedure

The system of the flow equations is solved numerically on three dimensional unstructured grid; a general in house developed fluid solver capable of handling unstructured meshes which has numerical cells with an arbitrary number of faces is used; this permits the handling of locally refined regions of particular interest. In the present study hexahedron computational cells are used; adaptive local grid refinement technique is used in order to enhance accuracy of the predictions in the areas of interest (i.e the liquid–gas interface), whilst maintaining the computational cost low, Theodorakakos and Bergeles [29]. The high-resolution differencing scheme CICSAM, proposed by Ubbink and Issa [30] is used in the numerical solution of the transport equation for α (VOF-variable). The discretization of the convection terms of the velocity components is based on a high resolution convection–diffusion differencing scheme (HR scheme) proposed by Jasak [31]. The time derivative was discretized using a second-order differencing scheme (Crank–Nicolson). To account for the high flow gradients near the free surface-interface, the cells are subdivided into a number of resolution levels in either sides of the free surface. As a result, the interface always lies in the densest grid region. A new locally refined mesh is created every 20 time steps for the cases that will be presented afterwards. In most cases 3 levels of adaptive local grid refinement are used. When a new grid with 1 level of local refinement is created an initial cell is split into eight secondary cells (for three dimensional problems). This technique results in a very dense grid resolution in the regions of interest, achieving time efficient computations on the dynamically adaptive grid compared to the equivalent fine resolution uniform grid; the local grid refinement technique in the interface region successfully kept the arithmetic error of mass conservation during the computations below 0.02%, in contrast to other methods in which errors in mass conservation were high, as reported in the literature, Pan and Suga [32]. The Flow solver has been successfully employed previously to predict similar cases, as that of a droplet impinging on a film, or on a hot substrate coupled with evaporation, Nikolopoulos et al. [33], Theodorakakos and Bergeles [29], Strotos et al. [34].

4. Numerical details of the simulated cases

The main parameters of the non-central binary collision process are the droplet diameter D_o and its initial impact velocity U_o; other significant parameters are the density ρ and viscosity μ of the liquid and gas phases as also the surface tension σ. These variables are grouped in dimensionless parameters, namely the Weber (We) and the Reynolds numbers (Re). For the off-centre droplet collision the most pertinent parameter is the impact parameter, Fig. 1.

The computational domain is shown in Fig. 1. The base grid and three levels of local grid refinement around the interface are shown. The distance between the droplets for the definition of the impact parameter is shown as also the position of the three planes ($X = 0.5X_{tot}$, $Z = 0.5Z_{tot}$ and $Y = 0$) on which results are presented. The experimental investigation reported by and Qian and Law [7] for two colliding droplets and for various Weber numbers and impact parameters form the basis of the present numerical simulation; the liquid phase is *n*-tetradecane and the gas phase nitrogen under environmental pressure. Three cases for droplet collision have been simulated; the parameters for which computations have been performed are given in Table 1.

In all cases the "base" grid employed consisted of 48,000 cells. The numerical simulation for case A, has lasted for 1 ½ month on a Pentium 4 2.4 GHz, 1 Gb Ram personal computer, while for cases B and C for 3 weeks (the simulated real time is less).

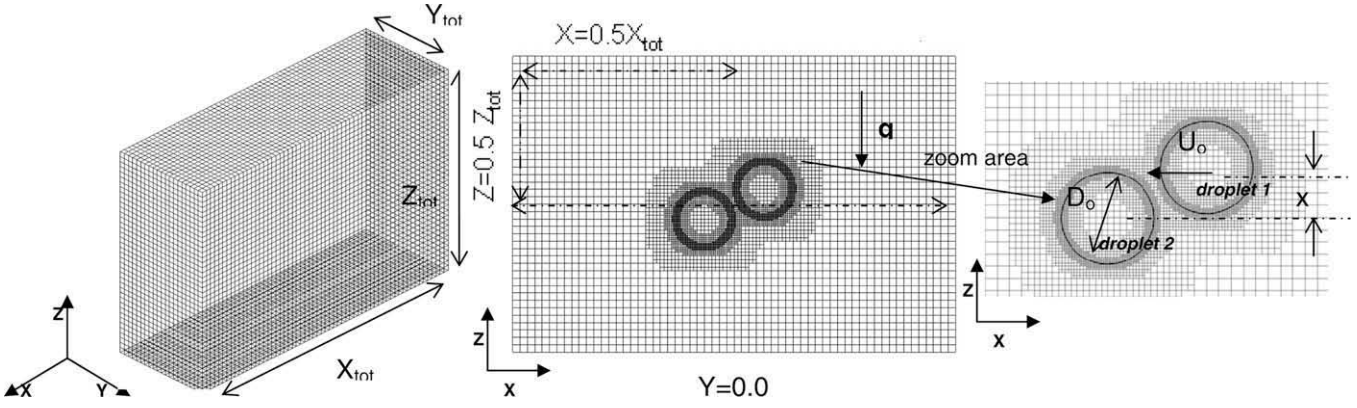

Fig. 1. The computational domain.

Table 1
Test cases examined.

Case	We	Re	B	D_o (μm)	Solution domain (X_{tot},Y_{tot},Z_{tot})	Base grid
A	70.8	327.7	0.25	356	$8D_o \times 2.67D_o \times 5.34D_o$	48,000 (and 3 levels of local grid refinement)
B	60.1	302.8	0.55	358	$7.96D_o \times 2.65D_o \times 5.3D_o$	48,000 (and 3 levels of local grid refinement)
C	60.8	313.7	0.68	380	$7.5D_o \times 2.5D_o \times 5D_o$	48,000 (and 3 levels of local grid refinement)

At the beginning of the calculations and starting with the base grid, after three levels of local grid refinement at the interfaces, each droplet is covered by 58,521 cells, whilst its interface by 35,926 numerical cells. The maximum refinement corresponds to a cell size of $D_o/60$. During the computations of all cases, the adaptive local grid refinement technique used, resulted in an maximum number of 227,886 computational cells, equivalent to 24,670,000 number of cells, if a uniform fine grid was used all over the computational domain, having the minimum grid size of the adaptive grid. The use of mirror boundary conditions allowed the simulation half of the droplets on the plane $Y = 0$. In mirror boundary conditions, the normal gradients of the velocity and of the α-variable are set to zero on the plane $Y = 0$. At the beginning of the simulation, $t = 0$, the droplets are $1.17D_o$ apart approaching each other with a velocity 2 U_o (relative velocity) (without any driving force acting on them), whilst the surrounding gas has zero velocity.

In order to investigate the grid dependency of the results, prediction of case B, using four levels of local grid refinement has been undertaken. Case B was selected for checking grid dependency as in this case a ligament is detached and a secondary droplet is formed, revealing the boundary of the governing physics between cases A and C. The numerical investigation of case B with four levels of local grid refinement was done up to time $t = 1.70$ ms investigating the effect of local refinement up to the critical stage of ligament pinching.

The finer mesh resulted in a two times denser grid at the region of the droplet interface, as compared to three levels of local grid refinement, with the maximum refinement corresponding to a cell size of $D_o/120$. The obtained results with the finer mesh were in accordance with the corresponding ones using three levels of local refinement as far as the general evolution of the phenomenon is concerned, (see Fig. 6, $t = 0.09$, $t = 0.13$, $t = 0.5$, $t = 1.3$, $t = 1.44$ and $t = 1.70$ ms) but minor differences existed at the time of ligament pinch off from the boundary droplets in the shape of the detached ligament at about time $t = 1.44$ ms as its edges are predicted to be more spherical using four levels of local refinement. However, again one secondary droplet was formed of almost the same size. Quantitatively the predicted elongations of the coalesced mass (L_1, defined in Fig. 6) using three and four levels of grid refinement are within less than 5% agreement, whilst the dimensions (L_2, w_2 defined in Fig. 6) of the satellite droplet and the ligament are predicted within an accuracy of 6.7%, as it is shown in Table 2, except for time $t = 1.44$ ms, i.e. at the moment of ligament pinch off; thus, the hydrodynamics does not seem to be significantly dependant on the level of mesh refinement. However, the maximum induced gas and liquid velocities at the time of first droplet contact differ about 20% with this difference becoming much smaller at subsequent times, thus confirming indirectly Pan and Kazuhiko [25] finding that the mechanism of bouncing collision is governed by the macroscopic dynamics while the mechanism of coalescence is related to the microscopic dynamics; trying to simulate the latter, a grid independent solution cannot be obtained as the phenomenon at the micro scale level is governed by non-continuous fluid dynamics equations and it is rather beyond our local grid refinement methodology.

5. Presentation and discussion of the results

5.1. Stability of collisions

The stability of the collisions has been a major point of interest in research since the early work by Adam et al. [1]. A number of papers on the stability of binary droplet collisions have been published, from which different descriptions of the stretching separation of the colliding droplets emerged. The first author who reported a mathematical equation for the definition of the critical impact parameter separating stretching separation from permanent coalescence was Park [2]. He derived an equation, balancing the surface tension forces in the region of contact between the water droplets with the forces due to angular momentum. Brazier-Smith et al. [3], assuming that separation will occur if the rotational energy of the complex droplet exceeds the surface energy required to reform the two water droplets from a coalesced nominal droplet produced an equation for the critical impact parameter. Arkhipov et al. [11] using the minimum potential energy variational principle by equating to zero the first variation of the potential energy of the system in a coordinate system rotating with constant angular velocity, obtained also a relation for the boundary between the stretching separation and coalescence (for water droplets). For propanol-2 droplets, Brenn et al. [10] performed a thorough experimental investigation and derived a mathematical expression for the definition of the critical impact parameter.

A comparison between the critical value of the impact parameter B predicted by the theoretical models and the corresponding values of the simulations (and the experiments of Qian and Law [7]), for the three cases examined is presented in Table 3. From the table is evident that for the first case the critical value of B for all models is above the corresponding value B of the simulation, while for the other two cases stands the opposite. As a result, for case A permanent coalescence, while for cases B and C stretching separation is anticipated. This is confirmed not only by the experiments of Qian and Law [7], but also by the present numerical results.

Table 2
Comparison of dimensions for case B using three and four levels of local refinement.

Time (ms)	% difference in L_2/R_o	% difference in w_2/R_o
0.86	0.49	4.88
1.31	−6.30	−2.27
1.44	−2.39	−30.23
1.55	2.05	−10.34
1.70	0.00	−7.69

Table 3
Calculation of the critical impact parameter B_{cr}, by various models for cases A, B and C.

Case	Park (1970)	Brazier-Smith et al. (1972)	Arkhipov et al. (1983)	Brenn (2001)	Value of B in simulation
A	0.45	0.30	0.41	0.38	0.25
B	0.46	0.32	0.45	0.42	0.55
C	0.42	0.32	0.44	0.42	0.68

5.2. The simulated cases

5.2.1. Coalescence of two droplets, case A, medium We number, low impact parameter (case A, Table 1 and Fig. 2, We = 70.8 and B = 0.25)

From the physical point of view, the criterion which determines droplet bounce or coalescence in droplet collisions is whether the intervening layer of the gas between the droplets can be squeezed off, so that the inter-droplet gap to be reduced to a dimension comparable to that of the molecular interaction, typically of the order of 10^2 Å, Mackay and Mason [35], Bradley and Stow [36]. As the two droplets approach each other, in the bouncing regime, high pressure is built up in the gap between the two droplets, while this pressure build-up causes the droplets to flatten. When bounce occurs, the droplets lose all of their kinetic energy, trying to expel the gas-layer. During the process of collision, kinetic energy is mainly transformed into surface energy.

After completing a wide range of experiments for *n*-tetradecane droplets in nitrogen environment under atmospheric pressure, Qian and Law [7], determined the critical *Weber* number, as a function of the impact parameter *B*, above which separation occurs. The combination of impact parameter *B* and We number characterizing case A (Table 1), is such that, according to Qian and Law [7], the two droplets are expected to coalesce permanently, without subsequent formation of any satellite droplets. This is also verified by the stability nomogram of Brenn et al. [10] and it is confirmed by the present numerical results.

Fig. 2 shows a sequence of photographs from the present simulation for the two colliding droplets and comparison with the experiments of Qian and Law [7] for the same angle of view. The extent of deformation and the shape of the two colliding droplets at various time instants after contact deduced from the experimental and numerical data are in reasonable agreement. Quantitative results were obtained by digitizing the photographs of [7] up to time $t = 0.95$ ms and the maximum elongation of the coalesced mass as defined in Fig. 2, Figs. 6 and 8 (maximum elongation of coalesced mass L_1) was calculated within an accuracy of 0.15 R_o.

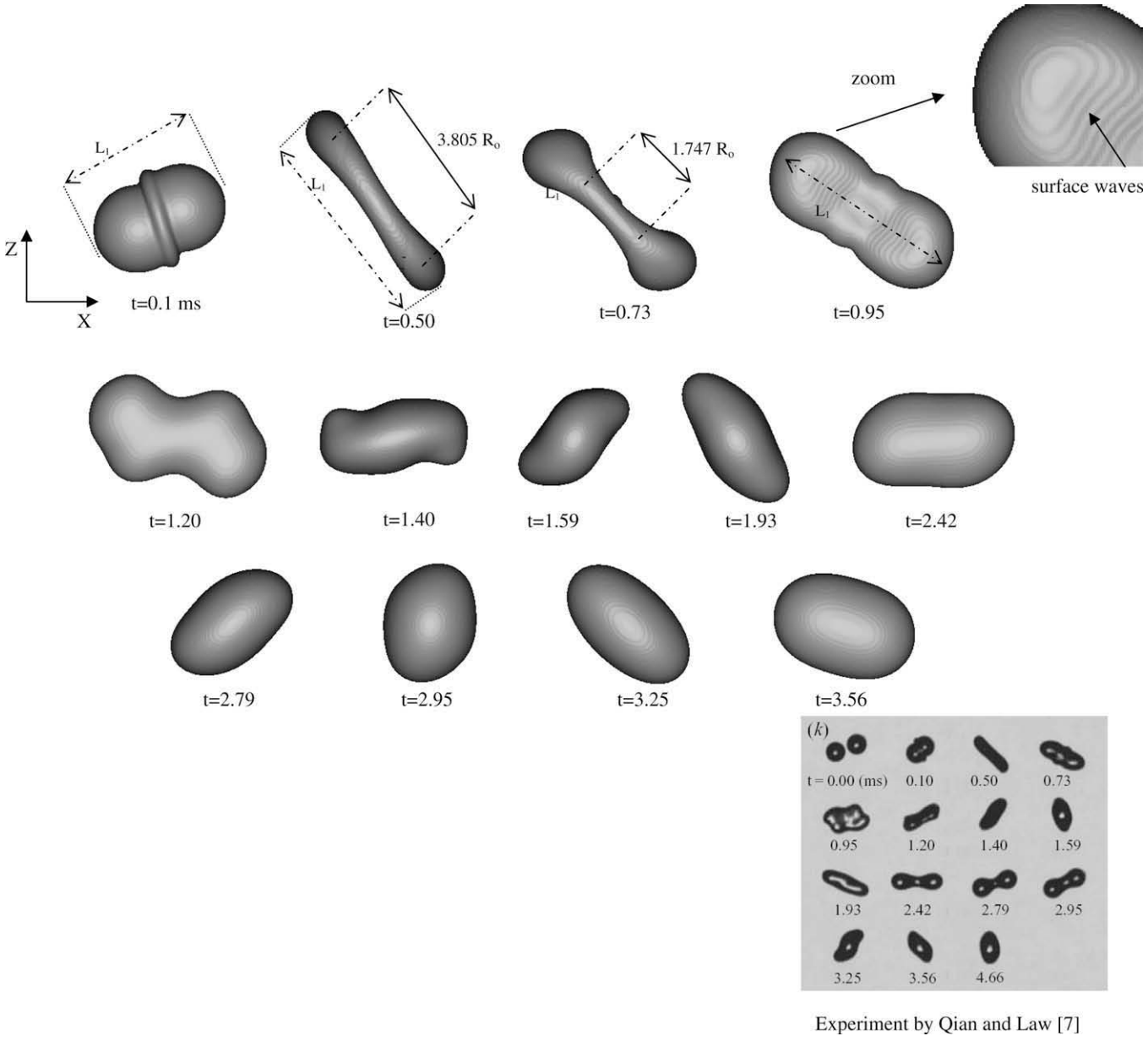

Fig. 2. Time evolution for the two colliding droplets, case A (view angle XZ plane), (We = 70.8, Re = 327.7, *B* = 0.25).

Table 4a gives the values of L_1 as deduced from the experiments and the corresponding simulation. The numerical predictions are in a good agreement with the experimental results.

As the droplets approach each other, the droplets are flattened in their contact region, Fig. 2, $t = 0.1$ ms and we assume that they merge; the merged mass, continues to deform in such a way as to form a donut shape (Figs. 2 and 3, $t = 0.5$ ms), with a thin film disc at the interior. At the junction of the thin film disc with the boundary ring a neck is formed and high liquid velocities develop, Fig. 4, $t = 0.5$ ms; due to lower pressure in the region, a high curvature surface is formed (Fig. 3, $t = 0.5$ ms), which is the seat of pinch off of the inner layer disc from the boundary ring (Fig. 3, $t = 0.52$ ms). This can be seen from the holes created at the internal periphery at the base of the boundary ring (Fig. 3, $t = 0.53$ ms), leading finally to the separation of the internal layer from the boundary ring. The internal disc like layer is transformed into a ligament, (Fig. 3, $t = 0.56$ ms), which elongates towards the Z-axis, (Fig. 3, $t = 0.58$ ms) but at latter stages, due to surface tension effects, recedes towards the centre of impact changing its elongation along the Y-axis, (Fig. 3, $t = 0.69$ ms) on the YZ plane. At time $t = 0.72$ ms (Fig. 3) the ligament elongates and bridges the inner edges of the external ring, merging with it and receding towards the symmetry plane; this process is completed at about time $t = 0.90$ ms, Fig. 3. The merged mass rotates around the Y-axis, Fig. 2, $t = 1.2$ ms, deforming into an oval shape elongating either in the symmetry plane, (Fig. 2, $t = 1.40$ ms), or in the XY plane (Fig. 2, $t = 1.59$ ms). At about time $t = 2.95$ ms and up to the final stages of impact, the merged droplet continues to oscillate around a spheroid shape, Fig. 2, $t = 3.56$ ms.

As the droplets approach each other, high pressure is built up in the gap; the droplets are flattening and conversion of the droplet kinetic energy into surface tension energy is taken place and gas is squeezed out in a form of a jet sheet; surrounding gas is entrained into the jet as it can be seen by the two rotating vortices at the edges of the jet, Fig. 4, time $t = 0.1$ ms. During this period of first contact the velocity of the squeezed gas out, takes a maximum value of around 829% of the initial droplet velocity with the liquid velocity at 321%; the maximum pressure is equal to around 79% of the kinetic energy of the droplet (based on the relative velocity of droplets); also at this period of contact small gas bubbles are trapped within the liquid phase having a very small volume of around 0.012% of the initial volume of both droplets (Fig. 5(a)).

Table 4a
Comparison of coalesced mass elongation between experimental data and simulation for case A.

Time	L_1/R_o (simulation)	L_1/R_o (experiment)
0.10	3.19	3.08
0.50	4.94	4.55
0.73	4.86	4.86
0.95	4.86	4.54

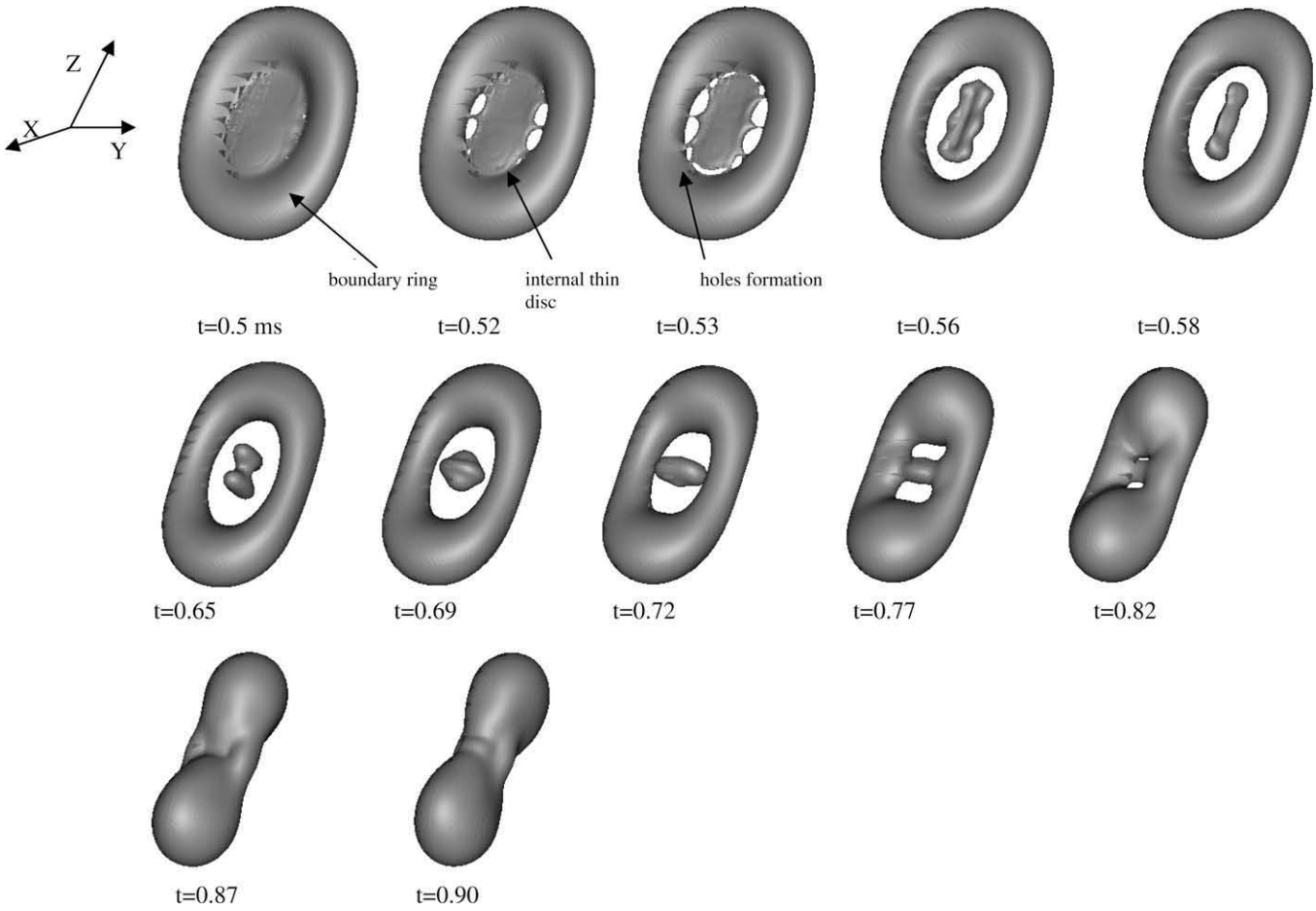

Fig. 3. Details of the time evolution of the "donut" shape formation of the two colliding droplets for case A, (We = 70.8, Re = 327.7, $B = 0.25$).

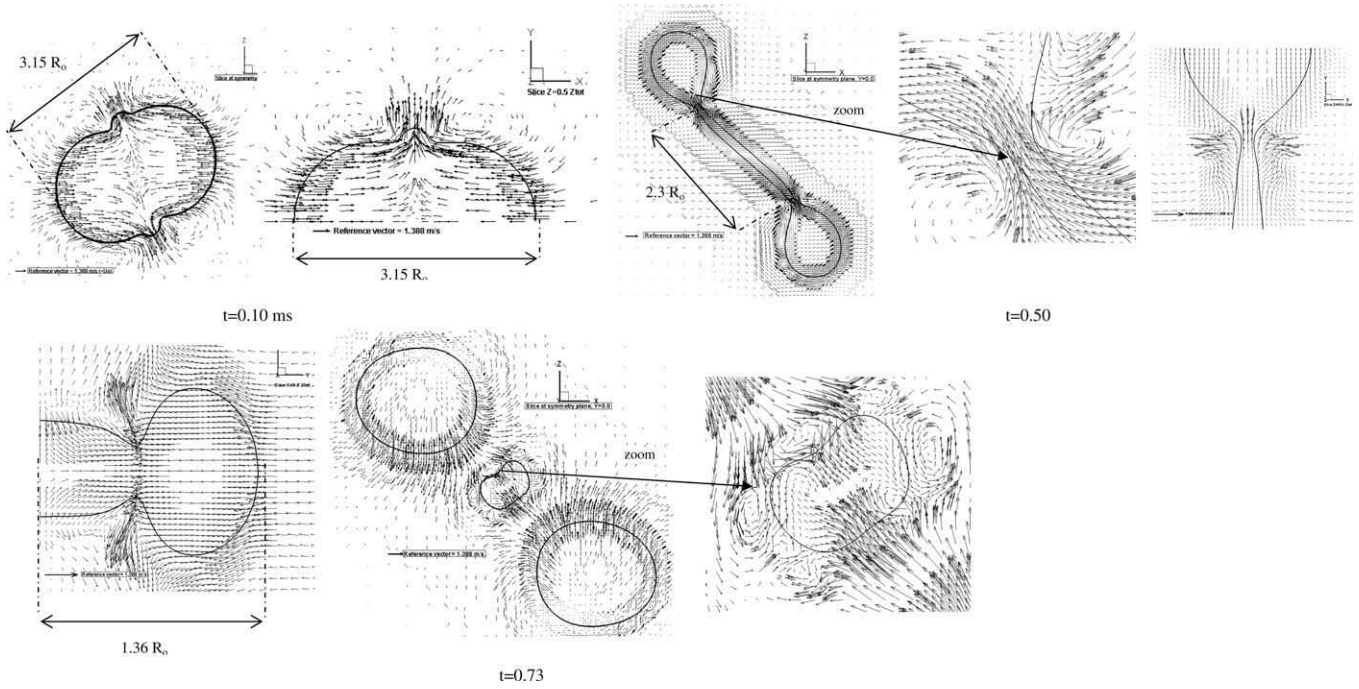

Fig. 4. Velocity field for case A at different times, (We = 70.8, Re = 327.7, B = 0.25).

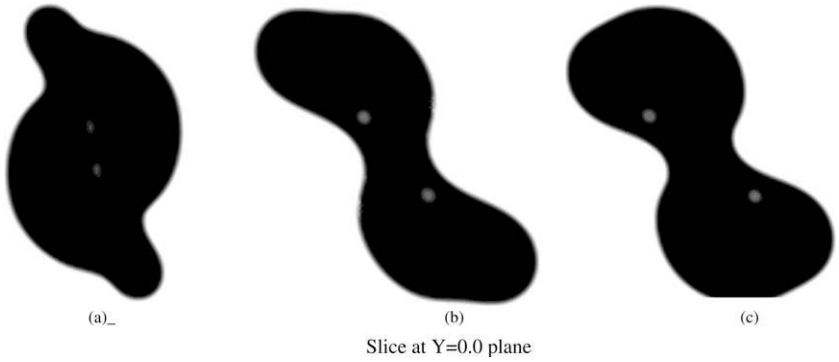

Fig. 5. Gas bubbles (white spots) inside the merged droplet, for cases (a) A, (b) B and (c) C, (A: (We = 70.8, Re = 327.7, B = 0.25); B: (We = 60.1, Re = 302.8, B = 0.55); C: (We = 60.8, Re = 313.7, B = 0.68)).

5.2.2. Stretching separation of two droplets, case B, medium We number, high impact parameter (case B, Table 1 and Fig. 6, We = 60.1, Re = 302.8, B = 0.55)

Case B, is characterized by a lower *We* number but by a higher impact parameter B compared to case A; Qian and Law [7] experiments indicate stretching separation; stretching separation is also predicted by the nomogram of Brenn et al. [10], with the formation of one satellite droplet. Stretching separation is also confirmed by the present numerical solution.

Fig. 6 presents a time sequence of predicted shapes of droplet collision for case B and the corresponding photographs of Qian and Law [7], for the same view angle. Table 4b gives the values of the maximum elongation of the coalesced mass, defined in Fig. 6, deduced from the photographs of [7] after digitization and the present predictions the agreement is again quite good, as in the previous case.

The two droplets coalesce after their initial contact; the merged mass deforms to an elliptical disc having a hole at the middle; the disc has a rotational motion around the Y axis (Fig. 6, t = 0.5 ms), which causes the merged droplet to stretch out and to create an elongated ligament type shape. After time t = 0.62 ms the central hole disappears as the merged mass shrinks in the Y direction, forming a cylindrical ligament connecting two boundary droplets (Fig. 6, t = 0.86 and t = 0.97). The merged mass, from its initial formation until the ligament's break up, rotates almost 150° at Y = 0 plane, (Fig. 6, t = 1.31 ms). The complete process of the collision and the satellite droplet formation is well captured by the simulation, except for two facts. First, the predicted ligament pinch off from the boundary droplets

Table 4b
Comparison of coalesced mass elongation between experimental data and simulation for case B.

Time	L_1/R_o (simulation)	L_1/R_o (experiment)
0.09	3.76	3.88
0.13	3.38	4.09
0.50	5.83	5.35
0.62	6.70	6.54
0.86	8.11	8.02
0.97	8.43	8.31

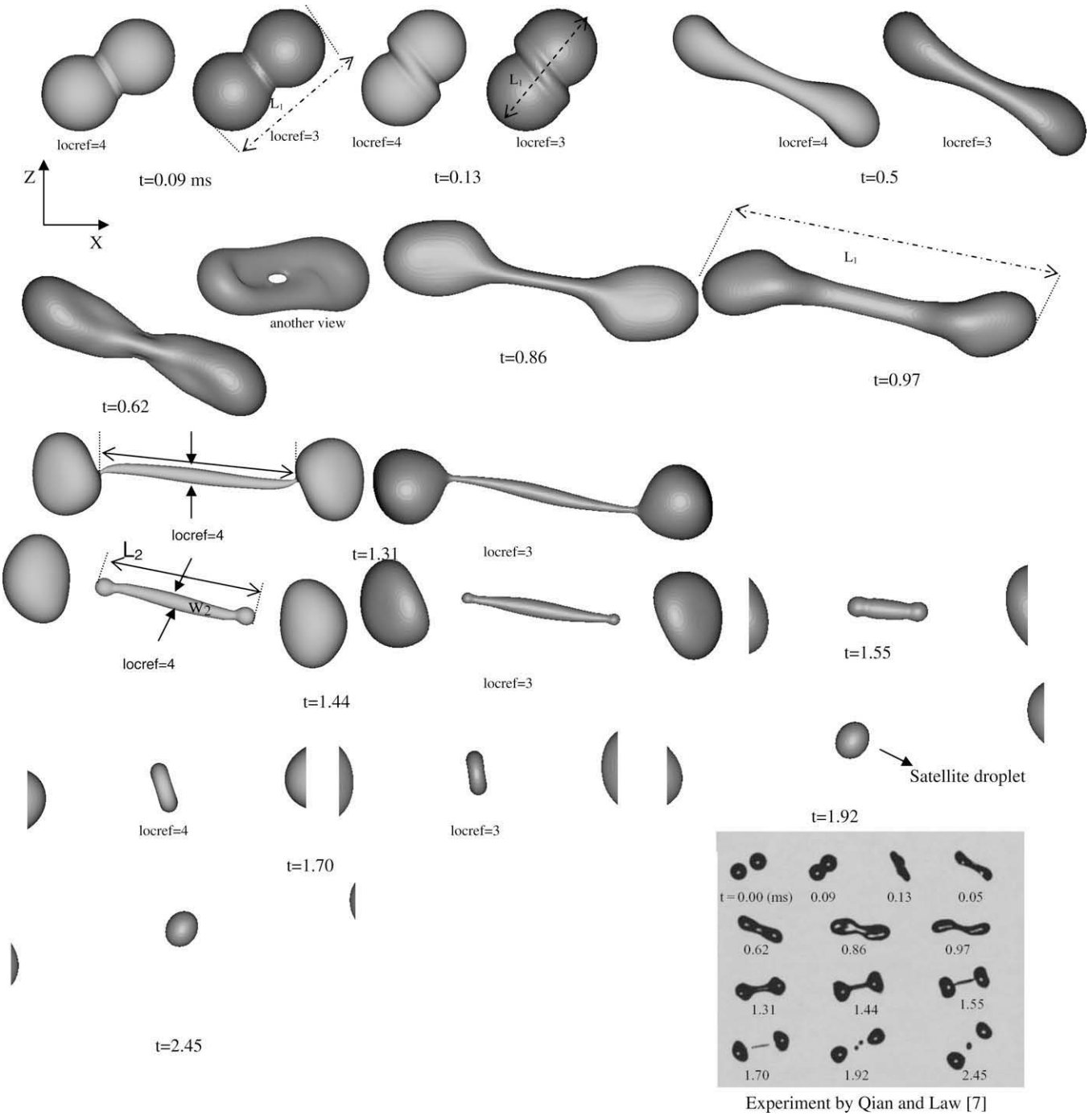

Fig. 6. Time evolution for case B using three and four levels of local refinement (view angle XZ plane), (We = 60.1, Re = 302.8, $B = 0.55$).

happens a little earlier than the experiments suggest (Fig. 6, $t = 1.44$ ms) and secondly according to the experimental image at $t = 1.92$ ms two satellite droplets are formed, which coalesce at $t = 2.45$ ms. This is not verified by the present numerical results, as after the time of ligament's separation from the boundary droplets, the ligament recedes into forming one satellite droplet. The volume of the satellite droplet is equal to 4.7% and the volume of each boundary droplet equal to around 47.6% of the initial volume of both droplets. The diameter of the satellite droplet is equal to 0.455 of the initial droplet, a value which is 10% lower than the experimental results of Brenn et al. [10]. The three droplets continue to oscillate in shape approaching an almost spherical shape (Fig. 6, $t = 1.70$, $t = 1.92$ and $t = 2.45$).

In Fig. 7 the velocity field for case B is presented. The approach of the two droplets increases the pressure in the gas gap between the two droplets, deforms and flattens the droplet surface in the contact region and squeezes out the gas, creating a gas jet, originating from the impact's centre between the two droplets, (Fig. 7, $Y = 0.0$, $t = 0.09$ ms). Surrounding gas is entrained into the gas jet and on the two sides of the gas jet two vortex rings attached to the liquid surface of each droplet are formed (Fig. 7, $Z = 05Z_{tot}$, $t = 0.09$ ms). The merged droplet elongates on the symmetry plane creating a hole in the middle (Fig. 7, $t = 0.5$ ms). Subsequently, the merged droplet contracts back towards the symmetry plane fills in the hole and elongates on the symmetry plane creating an elongated cylindrical liga-

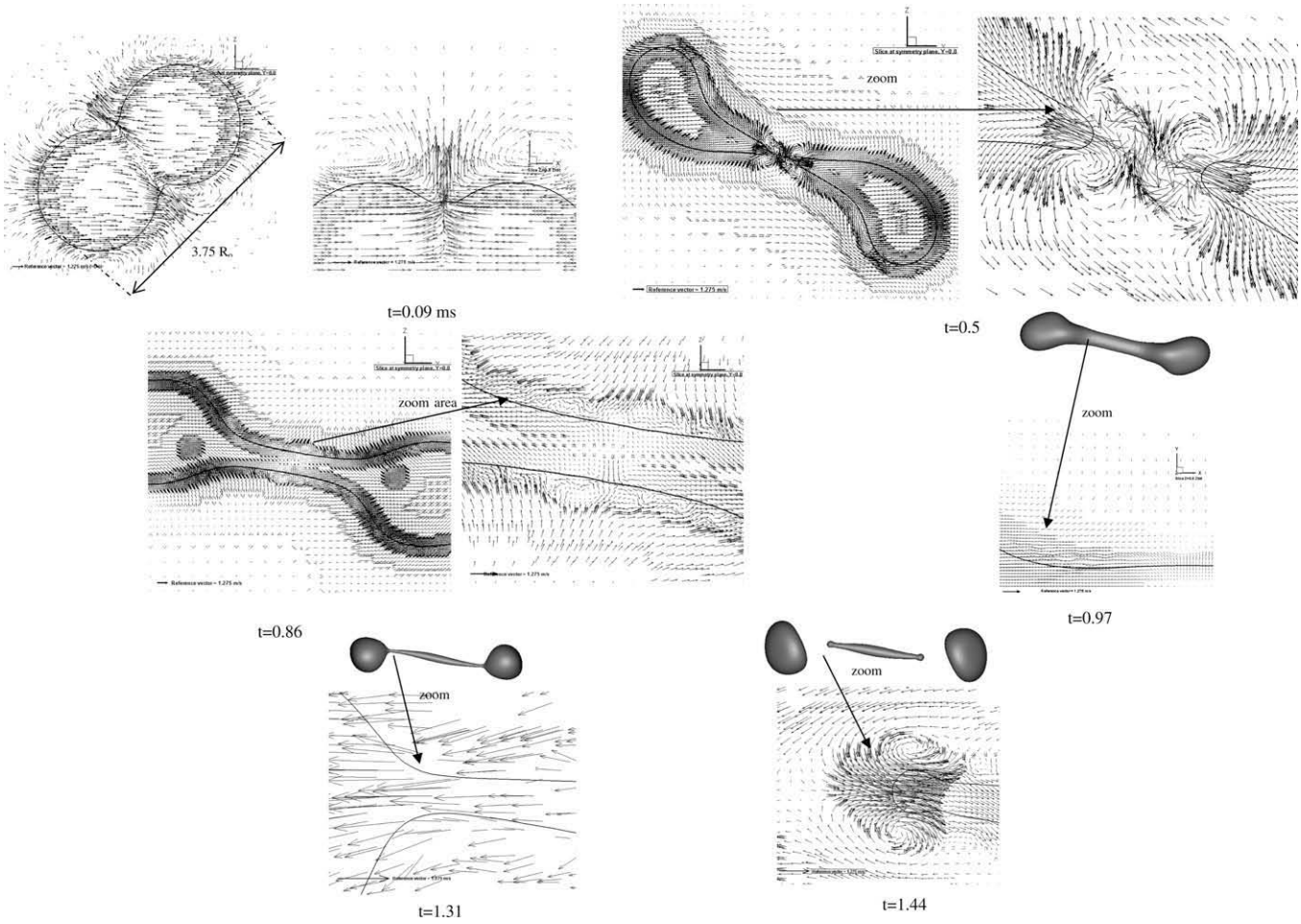

Fig. 7. Velocity field for case B at different slices, (We = 60.1, Re = 302.8, $B = 0.55$).

ment, in agreement with the experiments. Around this ligament, gas vortices with opposite direction to the initial ones formed during the initial stages of impact, exist. It is also of interest to observe that on the surface of the ligament, various organized flow instabilities occur (Fig. 7, $Y = 0.0$, $t = 0.86$ ms). As it has also been reported by Qian and Law [7], liquid flows towards the edges of the ligament (Fig. 7, $Z = 0.5Z_{tot}$, $t = 0.97$ ms), the ligament becomes thinner at the central region, mass accumulates at the edges creating boundary droplets and a neck similar to case A is formed (Fig. 7, $Y = 0.0$, $t = 1.31$ ms). The aforementioned ligament at about time, $t = 1.44$ ms, pinches off from the boundary droplets as it is also predicted by the corresponding experiment. Under the action of surface tension at the edges of the ligament, the flow reverses towards the ligament centre and the ligament is transformed following oscillations to a spherical shaped small droplet. The satellite droplet reaches an almost spherical shape at $t = 1.92$ ms (Fig. 6).

The value of the maximum gas jetting velocity at time of first droplet contact is equal to around 709%, whilst the corresponding liquid jetting velocity is equal to around 282% of the droplet's impact velocity. The maximum pressure developed is 62% of the initial total droplet's kinetic energy (based on the relative velocity of droplets). Gas bubbles are also trapped within the liquid phase and their volume is equal to around 0.023% of the initial volume of both droplets, i.e. almost double that of the corresponding value of previous case A (Fig. 5(b)).

5.2.3. Stretching separation of two droplets, case C, medium We number impact, very high impact parameter (case C, Table 1 and Fig. 8, We = 60.8, Re = 313.7, B = 0.68)

Case C, is characterized by slightly higher We number but by a much higher impact parameter B compared to case B. This case belongs to region of stretching separation leading to satellite droplet formation. For the present combination of Weber number and impact parameter Brenn's et al. [10] nomogram predicts the formation of one satellite droplet, whilst the experiments of Qian and Law [7] show three.

The merged mass, after coalescence of the two droplets, continues to deform from an initially rotating deformed ellipsoid (Fig. 8, $t = 0.15$) to the creation of two large liquid masses at the edges of an interconnecting flat ligament (Fig. 8, $t = 0.61$ ms). The line connecting the centre of masses of the two edge "droplets" rotates almost 143° at time $t = 1.51$ ms (Fig. 8, $t = 1.51$ ms) whilst the two boundary droplets are moving further apart being connected with an elongated but thinner ligament as in case B. However, the length of the ligament in the present case C is greater than case B at corresponding times and at the moment of ligament pinch off from the boundary droplets its length is 175.5% higher compared to case B. Simultaneously the width on the XZ plane is 87% and on XY plane 86%, of the corresponding values for case B, (Fig. 8, $t = 1.51$ ms and Fig. 10(a)–(c)). The complete process of the collision is well captured by the simulation compared to the experiments, despite the fact that the predicted droplet deformation is a little slower than the experiments suggest.

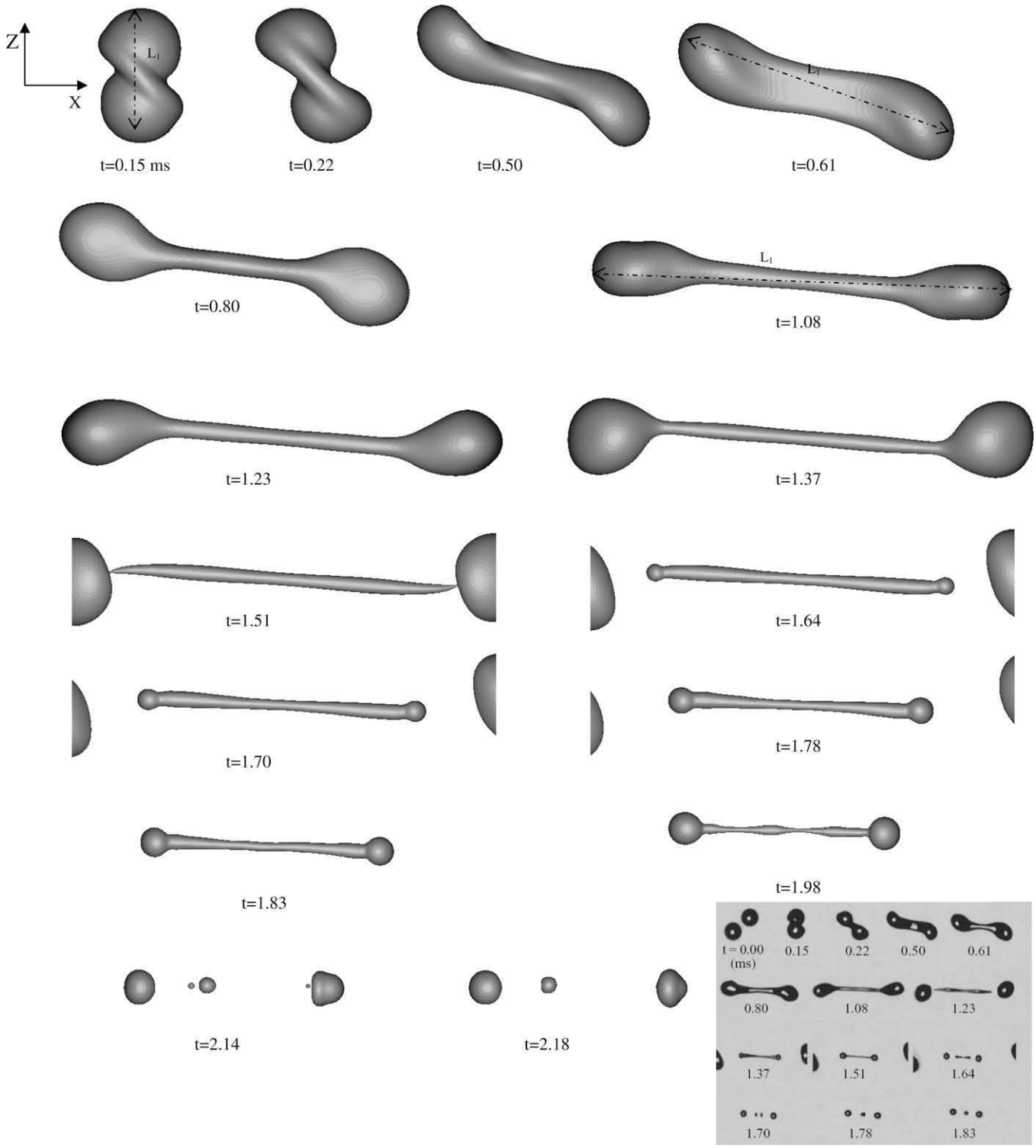

Fig. 8. Time evolution for case C (view angle XZ plane), (We = 60.8, Re = 313.7, B = 0.68).

Table 4c gives the values of the maximum elongation of the coalesced mass L_1 (defined in Fig. 8) as computed after digitization of the photographs [7] and the corresponding simulation. The numerical predictions of the length of the coalesced mass agrees quite well with experimental elongation.

The ligament breaks up into five satellite droplets (Fig. 8, t = 2.14 ms) and finally into three, as the smallest satellite droplets coalesce with the large neighbor ones (Fig. 8, t = 2.18 ms) in agreement with the Qian and Law [7] experiments. The volume of the first satellite droplet is equal to 3.3%, the second equal to 0.36%, the third equal to around 3% and either of the boundary droplets equal to around 46.67% of the initial volume of both droplets. The corresponding diameters of the first satellite droplet is equal to 0.404 (the experimental data give a value of 0.39), of the second satellite droplet is equal to 0.194 (the experimental data give a value of 0.15) and of the third equal to 0.391 (the experimental data give a value of 0.39), of the initial droplet diameter. The boundary droplets have diameters equal to around 98% D_o.

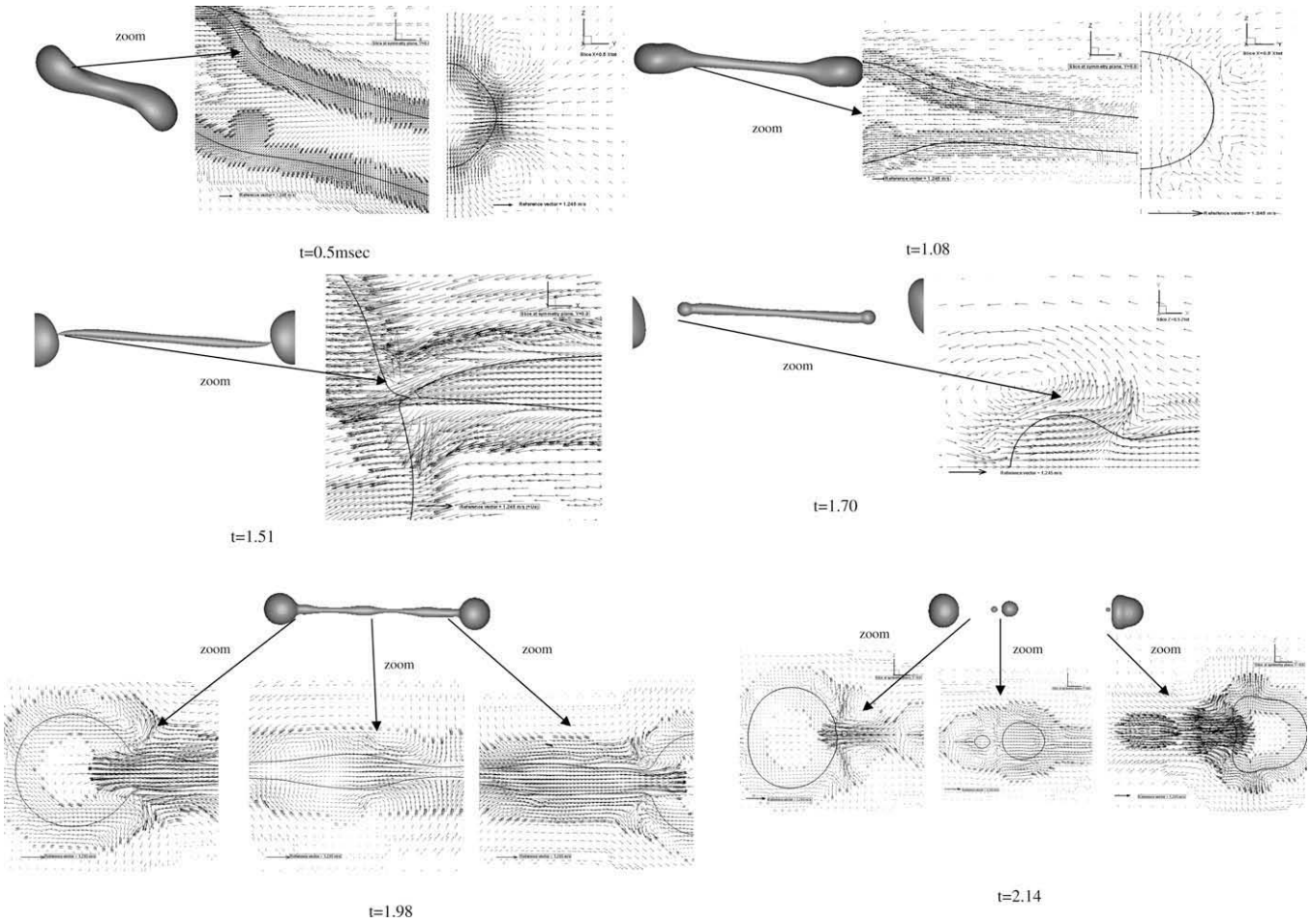

Fig. 9. Velocity field for case C at different slices, (We = 60.8, Re = 313.7, B = 0.68).

In Fig. 9 the induced velocity filed for this case is presented. As in case B the two droplets coalesce after their contact, squeezing out the gas, creating a gas jet sheet between the two droplets. The value of the maximum gas jetting velocity is equal to around 697%, whilst the corresponding liquid jetting velocity is equal to around 258% of the droplet's impact velocity. The maximum pressure developed is 100% of the initial total droplet's kinetic energy (based on the relative velocity of droplets). The previous velocities and pressures are in close agreement with the corresponding values for case B, indicating the similarity of the collision process at high impact We numbers. Gas bubbles are also trapped within the liquid phase but their volume is equal to 0.0260% of the initial volume of both droplets, i.e. almost equal to the corresponding value of case B (Fig. 5(c)).

At time t = 0.5 ms (Fig. 9, Y = 0.0) the ligament has already been formed with an increasing width in the Z direction but decreasing in Y direction, as it can been seen from the direction of the velocity vectors at vertical middle plane $X = 0.5X_{tot}$. Contra-rotating vortex tubes attached to the ligament can also be seen. The oscillating character of the evolution can be seen at time t = 1.08 (Fig. 9), where the ligament has decreased in thickness in the Z direction, the velocity vectors have changed direction, the rotational direction of the vortex tubes attached to the ligament's surface have also changed, whilst the merged mass has undertaken a further rotation on the XZ plane. The liquid velocity within the ligament continues to be directed towards its edges, increasing the size of the boundary droplets, whilst a neck is formed at the ligament edges (Fig. 9, t = 1.51 ms). The liquid velocity at the neck becomes 239% higher than the initial droplet velocity (Fig. 10d); therefore low pressure is created in the neck region which leads to high surface curvature and finally to ligament pinch off from the boundary droplets. After the detachment of the ligament from the boundary droplets the liquid velocity vector changes direction at the edges and liquid is moving inwards whilst in the central part of the ligament the flow continues to move outwards to the edges. This opposing liquid motion creates a neck at the central part of the ligament and two necks at the edges of the ligament, Fig. 9, t = 1.7 ms. Due to the confrontation of these motions moving waves are developing on the surface of the ligament, Fig. 9, t = 1.98, which eventually break the ligament to four satellite droplets, two satellite droplets coming from the two necks at the edges of the ligament and the other two from the body of the ligament, Fig. 9, t = 2.14 ms.

6. Characteristics of the merged droplets

6.1. Linear dimensions

The droplets after impact either coalesce permanently (case A) or separate forming a ligament between two boundary droplets (cases B and C). Fig. 10 presents the dimensions of the merged droplets as they change with time, for the three cases A, B and C. In Fig. 10(a) and (b), the merged droplet's non-dimensional widths at the central part at Y = 0 (vertical plane) and $Z = 0.5Z_{tot}$ (horizontal plane) planes are presented; the width of the merged droplet at the horizontal plane (Fig. 10b) is related inversely to the impact parameter indicating that the energy of collision is transferred to

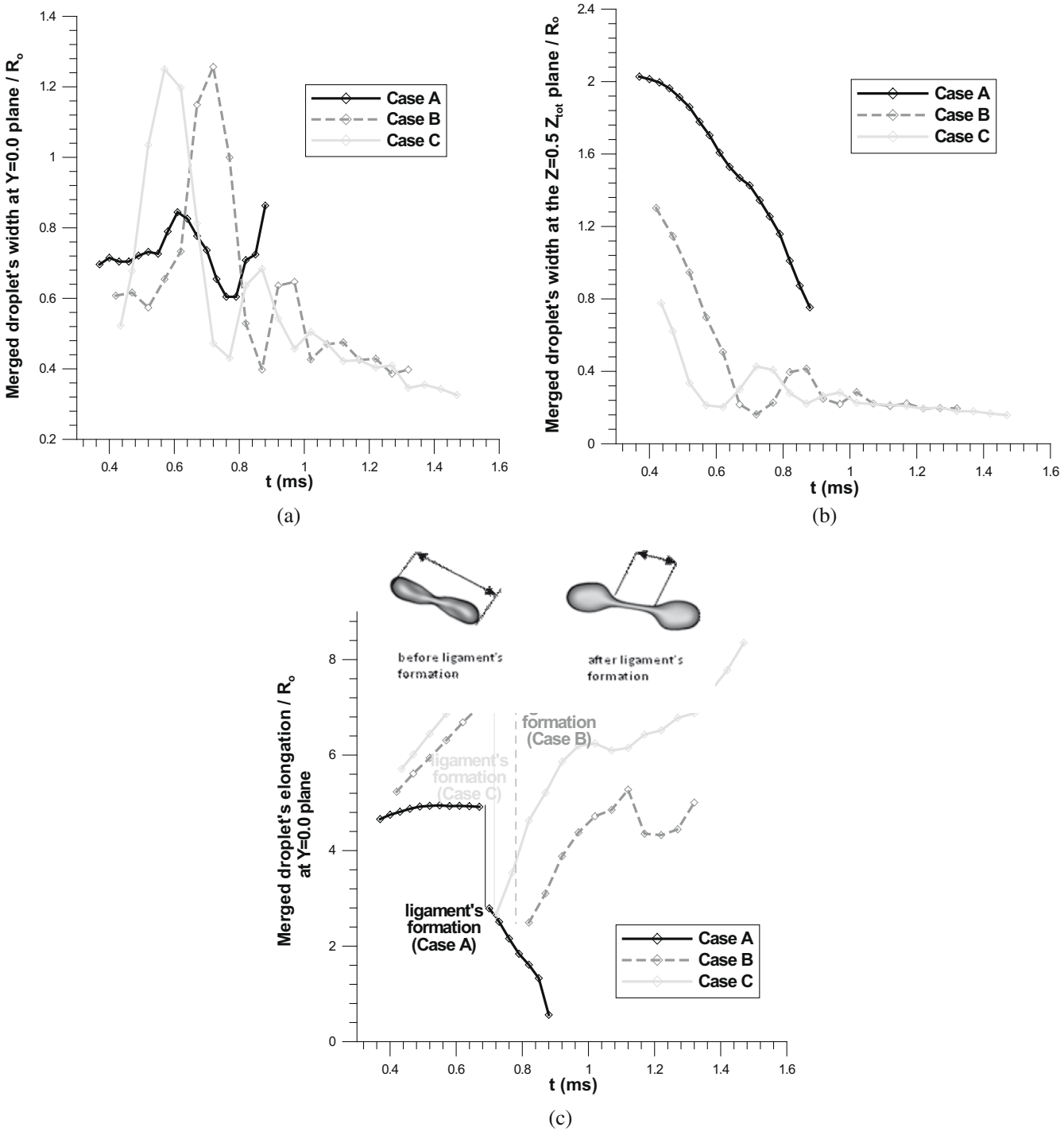

Fig. 10. Time evolution of basic merged droplet's for cases A, B and C, until ligament's detachment for cases B and C.

Table 4c
Comparison of coalesced mass elongation between experimental data and simulation for case C.

Time	L_1/R_o (simulation)	L_1/R_o (experiment)
0.15	3.35	3.54
0.22	3.63	3.93
0.50	6.28	6.17
0.61	7.27	7.44
0.80	8.87	9.27
1.08	10.40	10.74

the droplet extension in the lateral direction for small impact parameter; this width is reduced with time after $t > 0.4$ ms, monotonically for case A and in an oscillatory mode for cases B and C, (Fig. 10b). However the width of the merged droplets on the vertical plane for cases B and C is now larger compared to case A and reduces to nearly the same value (cases B and C) in an oscillatory way in the same phase with the width in the horizontal plane. The oscillations of these widths, for cases B and C are dumped out within few periods. The period of oscillation for cases B and C are well defined and it is approximately equal to 0.30 ms. At

times $t > 0.9$ ms, the widths of the merged droplet of case A are higher than those of cases B and C since in case A the droplets coalesce permanently, whilst in cases B and C a ligament starts to be formed. Fig. 10(c) presents the merged droplet's non-dimensional elongation on the vertical plane ($Y = 0$), which for case A decreases rapidly after the ligament's formation between the boundary droplets, at about time 0.65 ms after the impact, since the boundary droplets merge together. In contrast to case A, the ligament's length increases with time for cases B and C until satellite droplet formation. The ligament's elongation increases as impact parameter increases, case C versus case B and at the time of first satellite droplet formation the lengths of the two ligaments are 504%R_0 and 830%R_0, respectively. The non dimensional time (tU_o/D_o) from the time of droplet first contact to ligament pinch off and first satellite droplet formation is 4.48 and 4.73 correspondingly for cases B and C. Evidently, the time of ligament pinch off is roughly the same for the two cases B and C but in the latter case the ligament elongation is much higher compared to case B. The increased of impact parameter leads to the creation of a higher surface to volume ratio droplets, thus contributing to a higher combustion rate, in the case that binary collision between equal-sized droplets takes place in a burning environment.

6.2. Velocities and pressures

Fig. 11(a) presents the merged droplet's non-dimensional maximum liquid velocity on the vertical plane (symmetry plane $Y = 0$). This velocity is defined as positive if directed towards

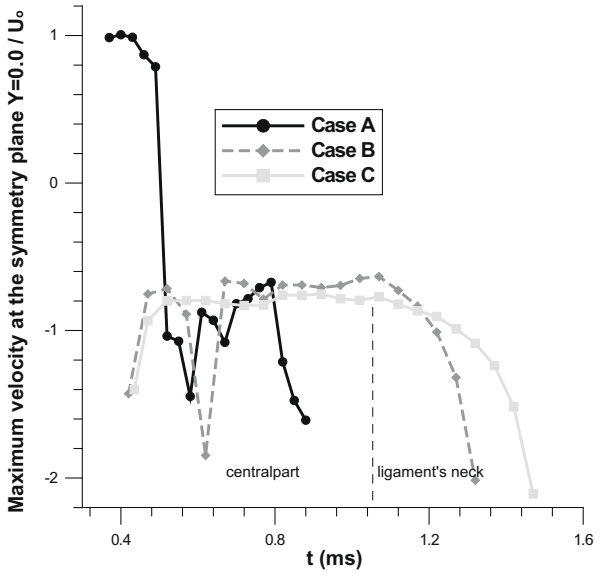

(a)

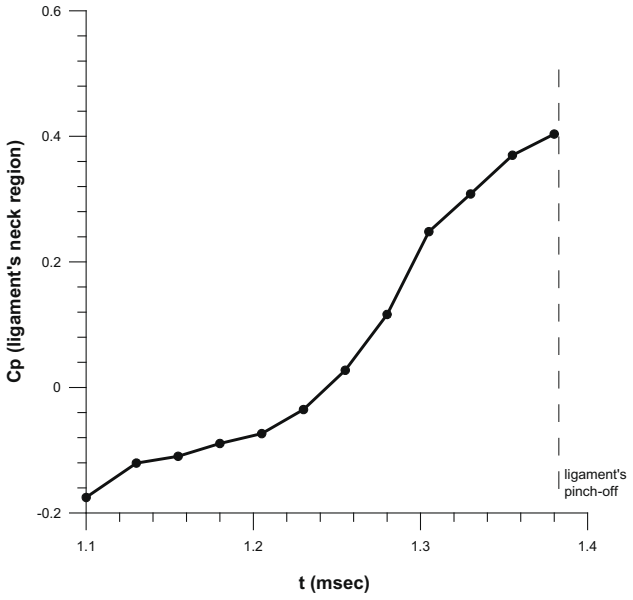

(c)

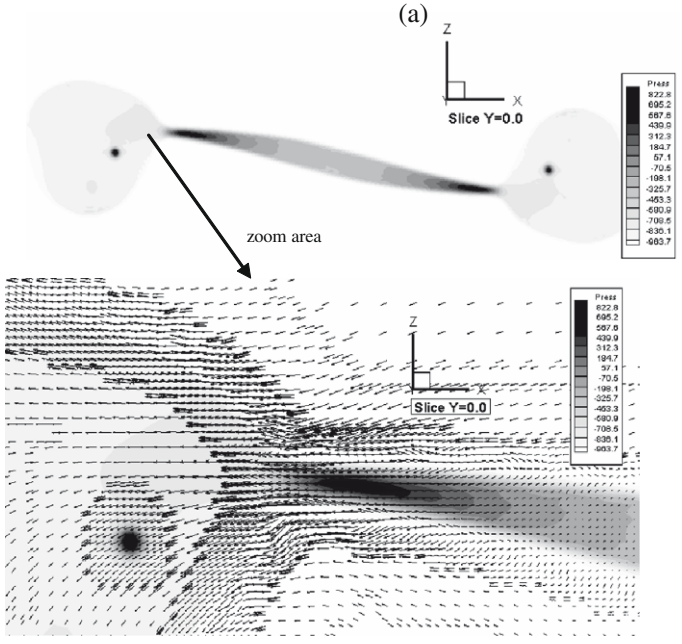

t=1.305 ms

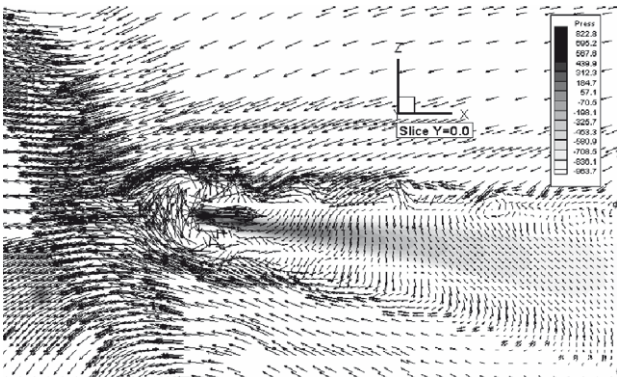

t=1.38

(b)

Fig. 11. (a) Time evolution of the maximum liquid velocity for cases A, B and C, (b) "end pinching" mechanism for case B and (c) time evolution of pressure at the ligament's neck region, (We = 60.1, Re = 302.8, $B = 0.55$).

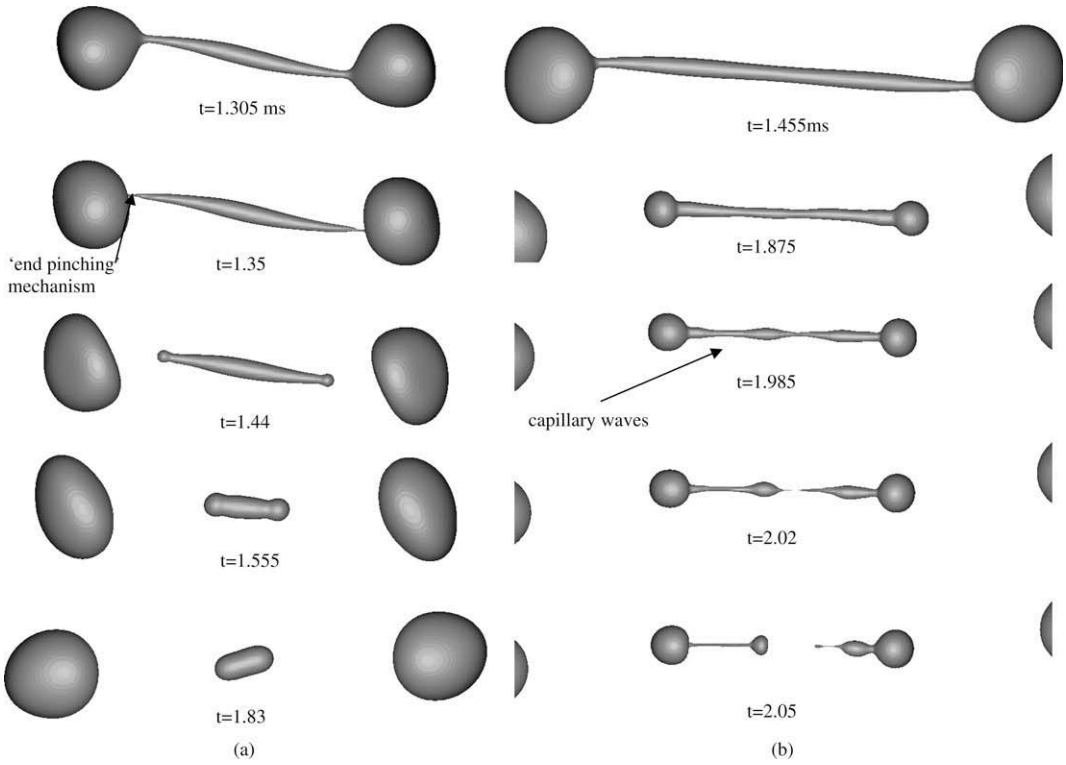

Fig. 12. Stretching separation for cases (a) B and (b) C, (B: We = 60.1, Re = 302.8, $B = 0.55$); C: (We = 60.8, Re = 313.7, $B = 0.68$).

the centre of impact and as negative in the opposite direction. In case A, and in the initial stages of collision, the maximum velocity in the ligament is positive and brings the two droplets closer; at time around $t = 0.5$ ms, the velocity changes sign, obtaining a maximum value of $1.6U_0$ increasing the elongation of the boundary ring and with a tendency to separate the two droplets from coalescence; this maximum velocity is found in the central part of the merged droplets. In the other two cases, B and C, for which stretching separation is observed, the maximum liquid velocity in the ligament, is always negative; in the first stages of collision ($t < 1$ ms) maximum velocity is found in the central part of the ligament, but after this time at the ligament's neck and is approximately larger than $2U_0$, a velocity which is higher than the corresponding velocity for case A. For cases B and C, the maximum velocity is almost the same, until the ligament's spill off from the boundary droplets. Fig. 11(b) indicates the pressure distribution in the liquid phase, just before ligament pinch off from the boundary droplets, for case B. The flow is directed from the ligament centre towards the edge droplets being decelerated and an area of maximum pressure is formed before the seat of the pinch off; after that a strong flow acceleration exists between the high pressure area and the low pressure inside the boundary droplets (leading to maximum velocity) and low pressure is formed at the seat of ligament pinch off; after the ligament's pinch off the flow reverses moving from the high pressure area at the edge of the ligament towards the centre, but the flow from the centre of the ligament continues to move towards the ligament edges; the two opposing motions create capillary waves, (as it can be seen in Fig. 11(b), $t = 1.38$ ms). The capillary waves combined with the increased length to diameter ratio of the ligament for case C lead to the formation of more than one satellite droplets. The maximum pressure inside the ligament for cases B and C is continuously increasing with time as shown in Fig. 11c for case B.

Finally, Fig. 12 presents a more detailed qualitative description of the two main mechanisms identified in the present numerical investigation; the "end-pinching" mechanism in case B and the induced capillary waves in case C, due to the increased length to diameter ratio of the ligament for that case.

7. Conclusions

The flow development arising from the off-centre binary collision of two equal sized droplets was numerically studied using a finite volume methodology with the Volume of Fluid (VOF) technique; a recently developed local grid refinement methodology allowed the correct tracking of the interface of the colliding droplets. A higher order discretization scheme was used for the numerical solution of the transport equation for the VOF indicator in order to accurately track the droplet–gas interface. Two different mechanisms of satellite droplets formation by unstable binary collisions are identified. The first one referred by Qian and Law [7], called "end-pinching" mechanism and the second one due to capillary waves. The VOF method was capable of predicting details of the fine scales of the whole flow field, like gas bubble entrapment, maximum deformation, capillary waves, air and liquid jetting and satellite droplet formation. The effect of *Weber* number and impact parameter on the main characteristics of ligament was quantified and the predicted velocities and pressures developed within the ligament clarified further the mechanism of ligament pinch off.

Acknowledgment

The financial support of the EU under contract N° ENK6-2000-00051 is acknowledged.

References

[1] J.R. Adam, N.R. Lindblad, C.D. Hendricks, The collision, coalescence, and disruption of water droplets, J. Appl. Phys. 39 (1968) 173.
[2] R.W. Park, Behavior of Water Drops Colliding in Humid Nitrogen. PhD Thesis, Department of Chemical Engineering, The University of Wisconsin, 1970.

[3] P.R. Brazier-Smith, S.G. Jennings, J. Latham, The interaction of falling water drops: coalescence, Proc. R. Soc. Lond. A 326 (1972) 393.
[4] N. Ashgriz, J.Y. Poo, Coalescence and separation in binary collision of liquid drops, J. Fluid. Mech. 221 (1990) 183–204.
[5] G.M. Faeth, Current status of droplet and liquid combustion, Prog. Energy Combust. Sci. 3 (1977) 191.
[6] P.J. O'Rourke, F.V. Bracco, Modeling of droplet interactions in thick sprays and a comparison with experiments, Startified Charge Auto. Eng. Conf., 101–115 Inst. Mech. Eng. Pub. ISMB 0-85298-4693.
[7] J. Qian, C.K. Law, Regimes of coalescence and separation in droplet collision, J. Fluid Mech. 331 (1997) 59.
[8] Y.J. Jiang, A. Umemura, C.K. Law, An experimental investigation on the collision behaviour of hydrocarbon droplets, J. Fluid Mech. 234 (1992) 171.
[9] J.-P. Estrade, H. Carentz, G. Lavergne, Y. Biscos, Experimental investigation of dynamic binary collision of ethanol droplets – A model for droplet coalescence and bouncing, Int. J. Heat Fluid Flow 20 (1999) 486.
[10] G. Brenn, D. Valkovska, K.D. Danov, The formation of satellite droplets by unstable binary drop collisions, Phys. Fluids 13 (2002) 2463–2477.
[11] V.A. Arkhipov, I.M. Vasenin, V.F. Trofimov, Stability of colliding drops of ideal liquid, Zh. Prikl. Mekh. Tekh. Fiz. 3 (1983) 95.
[12] K.D. Willis, M.E. Orme, Experiments on the dynamics of droplet collisions in a vacuum, Exp. Fluids 29 (2000) 347–358.
[13] S.O. Unverdi, Numerical Simulation of Multi-fluid Flows. PhD Thesis, The University of Michigan, 1990.
[14] S.O. Unverdi, G. Tryggvason, A front tracking method for viscous incompressible flows, J. Comput. Phys. 100 (1992) 25.
[15] S.O. Unverdi, G. Tryggvason, Multifluid flows, Physica D 60 (1992) 70.
[16] M.R. Nobari, Y.J. Jan, G. Tryggvason, Head-on collision of drops – A numerical investigation, Phys. Fluids 8 (1996) 29–42.
[17] M.R. Nobari, G. Tryggvason, Numerical simulation of three dimensional droplet collision, AIAA J. 34 (4) (1996) 750–755.
[18] F. Mashayek, A. Ashgriz, W.J. Minkowycz, B. Shotornan, Coalescence collision of liquid drops, Int. J. Heat Mass Transfer 46 (2003) 77.
[19] B. Lafaurie, C. Nardone, R. Scardovelli, S. Zaleski, G. Zanetti, Modelling merging and fragmentation in multiphase flows with SURFER, J. Comput. Phys. 113 (1994) 134.
[20] P. Drtina, M. Schelkle, A. Frohn, Numerical simulation of droplet deformation and droplet coagulation applying lattice gas models, J. Aerosol Sci. 22 (Suppl. 1) (1991) S249–252.
[21] M. Schelkle, A. Frohn, Two dimensional lattice gas simulation of droplet deformation and non-central collisions, J. Aerosol Sci. 26 (Suppl. 1) (1993) 929–930.
[22] M. Schelkle, A. Frohn, Three-dimensional lattice gas simulation of binary collisions between equal droplets, J. Aerosol Sci. 26 (Suppl. 1) (1995) 145–146.
[23] M. Rieber, A. Frohn, Three-dimensional navier–stokes simulation of binary collisions between droplets of equal size, J. Aerosol Sci. 24 (Suppl. 1) (1995) 513–515.
[24] T. Inamuro, S. Tajima, F. Ogino, Lattice Boltzmann simulation of droplet collision dynamics, Int. J. Heat Mass Transfer 47 (2004) 4649.
[25] Y. Pan, S. Kazuhiko, Numerical simulation of binary liquid droplet collision, Phys. Fluids 17 (2005).
[26] A. Munnannur, R.D. Reitz, A new predictive model for fragmenting and non-fragmenting binary droplet collisions, Int. J. Multiphase Flow 33 (8) (2007) 873–896.
[27] C.W. Hirt, B.D. Nichols, Volume of fluid (VOF) method for the dynamics of free boundaries, J. Comput. Phys. 39 (1981) 201–225.
[28] J.U. Brackbill, D.B. Kothe, C. Zemach, A continuum method for modeling surface tension, J. Comput. Phys. 100 (2) (1992) 335–354.
[29] A. Theodorakakos, G. Bergeles, Simulation of sharp gas–liquid interface using VOF method and adaptive grid local refinement around the interface, Int. J. Numer. Method Fluids 45 (2004) 421–439.
[30] O. Ubbink, R.I. Issa, A method for capturing sharp fluid interfaces on arbitrary meshes, J. Comput. Phys. 153 (1) (1999) 26–50.
[31] H. Jasak, Error Analysis and Estimation for Finite Volume Method with Applications to Fluid Flows. PhD Thesis, Department of Mechanical Engineering, Imperial College of Science, Technology & Medicine, University of London, 1996.
[32] Y. Pan, K. Suga, Numerical simulation of binary liquid droplet collision, Phys. Fluids 17 (2005) 1–14.
[33] N. Nikolopoulos, A. Theodorakakos, G. Bergeles, Three-dimensional numerical investigation of a droplet impinging normally onto a wall-film, J. Comput. Phys. 225 (2007) 322–341.
[34] G. Strotos, M. Gavaises, A. Theodorakakos, G. Bergeles, Numerical investigation on the evaporation of droplets depositing on heated surfaces at low Weber numbers, Int. J. Heat Mass Transfer 51 (7–8) (2008) 1516–1529.
[35] G.D. Mackay, S.G. Mason, The gravity effect approach and coalescence of fluid drops at liquid interfaces, Can. J. Chem. Eng. 41 (1963) 203.
[36] S.G. Bradley, C.D. Stow, Collision between liquid drops, Philos. Trans. R. Soc. Lond Ser. A 287 (1978) 635.